Journal of Power Sources 249 (2014) 509–514

Contents lists available at ScienceDirect

Journal of Power Sources

journal homepage: www.elsevier.com/locate/jpowsour

Effect of interface modifications on voltage fade in $0.5Li_2MnO_3 \cdot 0.5LiNi_{0.375}Mn_{0.375}Co_{0.25}O_2$ cathode materials

Ira Bloom [a,*], Lynn Trahey [a], Ali Abouimrane [a], Ilias Belharouak [a], Xiaofeng Zhang [a], Qingliu Wu [a], Wenquan Lu [a], Daniel P. Abraham [a], Martin Bettge [a], Jeffrey W. Elam [b], Xiangbo Meng [b], Anthony K. Burrell [a], Chunmei Ban [c], Robert Tenent [c], Jagjit Nanda [d], Nancy Dudney [d]

[a] Chemical Sciences and Engineering Division, Argonne National Laboratory, 9700 S. Cass Avenue, Argonne, IL 60439, USA
[b] Energy Systems Division, Argonne National Laboratory, 9700 S. Cass Avenue, Argonne, IL 60439, USA
[c] National Renewable Energy Laboratory, 15013 Denver West Parkway, Golden, CO 80401, USA
[d] Oak Ridge National Laboratories, P.O. Box 2008, Oak Ridge, TN 37831, USA

HIGHLIGHTS

- The effects of coatings and electrolyte additives on voltage fade were investigated.
- Cells containing these materials were tested at room temperature.
- The coatings and additives studied had little-to-no effect on voltage fade.

ARTICLE INFO

Article history:
Received 24 June 2013
Received in revised form
7 October 2013
Accepted 10 October 2013
Available online 18 October 2013

Keywords:
Lithium-ion batteries
Composite cathode materials
Voltage fade
Coatings
Electrolyte additives

ABSTRACT

The effects of the coatings Al_2O_3, $LiAlO_x$, ZrO_2, TiO_2, $AlPO_4$, and LiPON and of the electrolyte additives 3-hexylthiophene and lithium difluoro (oxalato)borate (LiDFOB) on the voltage fade phenomenon in $0.5Li_2MnO_3 \cdot 0.5LiNi_{0.375}Mn_{0.375}Co_{0.25}O_2$ cathodes were investigated. Cells containing these materials or additives were cycled according to a standard protocol at room temperature between 2.0 and 4.7 V vs. Li^+/Li. As expected, the cells containing either an additive or a coated cathode displayed less capacity loss than cells containing an uncoated cathode and no additive. The voltage fade phenomenon was quantified in terms of changes in the average cell voltage (Wh/Ah). The results indicate that, within experimental error, all of the coatings and additives produced little-to-no effect on voltage fade.

1. Introduction

Because of their potential for high energy density, lithium-ion batteries have attracted much attention in applications as diverse as transportation and the electric power grid. Layered materials in the Li–Mn-rich portion of the Li–Ni–Mn–Co–O phase diagram are the focus of much development work because they display a reversible capacity density of more than 230 mAh g^{-1} [1] and consist mostly of Mn, a relatively inexpensive metal. The Li–Mn-rich, Li–Ni–Mn–Co oxides (LMR–NMC) are structurally integrated composites of Li_2MnO_3 and $Li(Ni,Mn,Co)O_2$ [1,2] and are usually denoted as $aLi_2MnO_3 \cdot (1-a)Li(Ni,Mn,Co)O_2$.

When cells containing LMR–NMC materials are cycled, however, their capacity declines, impedance rises, and the shape of the voltage vs. capacity curve changes [3]. Examples of these effects are given in Fig. 1a and b. As shown in Fig. 1a, the capacity of the cell decreases from ~270 to ~264 mAh g^{-1} with cycling, and there is a subtle decline of the discharge curve. This decline is more apparent when the voltage data in Fig. 1a are plotted against normalized capacity (Fig. 1b). A similar decline is also observed on charging, strongly suggesting that changes to the equilibrium electrochemical potential of the active material

* Corresponding author.
E-mail address: ira.bloom@anl.gov (I. Bloom).

0378-7753/$ – see front matter © 2013 Elsevier B.V. All rights reserved.
http://dx.doi.org/10.1016/j.jpowsour.2013.10.035

cause the voltage fade. In the literature, the continuous change in the shape of the discharge (and charge) curves has been attributed to the formation of a spinel-like phase [3–7]. As a result of the loss in potential, there is a loss in energy, limiting the utility of these materials in energy-demanding applications, such as in electric vehicles.

Three national laboratories, Argonne National Laboratory, the National Renewable Energy Laboratory and Oak Ridge National Laboratory, are collaborating to devise methods to arrest this voltage fade. The work, described below, approaches this goal by investigating the effects of using cathode coatings and electrolyte additives. In the literature, coatings, surface modifications, and additives of many descriptions have been used to stabilize the capacity of cathode materials and enhance cycling ability [2–39], enhance the rate capacity of cathode materials [10,11,13,17,18,20,21,29,40], lessen their thermal reactivity [9,41–44], lessen their reactivity towards the organic electrolytes [45], and promote secondary electrolyte interface layer formation on the cathode [43]. The effects of the coatings Al_2O_3, $LiAlO_x$, ZrO_2, TiO_2, $AlPO_4$, and lithium phosphorus oxynitride (LiPON) and of the electrolyte additives 3-hexylthiophene and LiDFOB on voltage fade were investigated. It should be noted that both electrolyte additives are very effective in forming a protective layer on the surface of the positive electrode at high potentials [26,38].

2. Experimental

All positive electrodes contained the same commercially available LMR-NMC material, $0.5Li_2MnO_3 \cdot 0.5LiNi_{0.375}Mn_{0.375}Co_{0.25}O_2$ (Toda Kogyo, Japan; referred to as HE5050), which was used to fabricate coated and uncoated cathode laminates.

2.1. Laminate coatings

Atomic-layer deposition (ALD) coatings of Al_2O_3, TiO_2, ZrO_2, and $LiAlO_x$ were applied to HE5050 laminate sheets (see below for the composition of the laminate), some of which were made by the Argonne Cell Fabrication Facility. These ALD coatings were deposited under nitrogen and were performed using 6 ALD cycles and had a thickness below 3 nm, as determined from previous studies. The time at temperature (120 °C) for 6 cycles averaged less than 30 min. The laminates were stored in an argon glovebox after coating. Cells were then made and cycled in duplicate.

2.1.1. Al_2O_3

Ultrathin films of alumina were grown directly on the laminated HE5050 electrodes. The precursors for the Al_2O_3 ALD coating were trimethylaluminium (97%, Aldrich) and H_2O (HPLC grade, Sigma–Aldrich). The coatings were obtained using the sequential and self-limiting surface reactions shown in (A) and (B) below [37,46–48].

$$\text{surface-OH} + Al(CH_3)_3 \rightarrow \text{surface-O–}Al(CH_3)_2 + CH_4 \quad \text{(A)}$$

$$\text{surface-O–}Al(CH_3)^* + H_2O \rightarrow \text{surface-O–}Al\text{–OH} + CH_4 \quad \text{(B)}$$

Each ALD cycle consisted of these two reactions. The typical growth rate for the Al_2O_3 coating was ~1.1 Å per cycle; however, the growth may be enhanced for the high-surface-area, torturous electrodes [48].

2.1.2. TiO_2, ZrO_2, and $LiAlO_x$

The ALD coating of TiO_2 was grown on the HE5050 laminate at both 100 °C and 150 °C using titanium tetraisopropoxide ($Ti(OCH(CH_3)_2)_4$, Sigma–Aldrich) and H_2O as precursors. The coating was obtained using the reactions shown in (C) and (D) below [49].

$$2\,\text{surface-OH} + Ti(OCH(CH_3)_2)_4\,(g) \rightarrow \text{surface-O}_2\text{–}Ti(OCH(CH_3)_2)_2 + 2(CH_3)_2CHOH\,(g) \quad \text{(C)}$$

$$\text{surface-O}_2\text{–}Ti(OCH(CH_3)_2)_2 + 2H_2O\,(g) \rightarrow \text{surface-O}_2\text{–}Ti(OH)_2 + 2(CH_3)_2CHOH\,(g) \quad \text{(D)}$$

The ALD coating of ZrO_2 was grown on the HE5050 laminate at both 100 °C and 150 °C using tetrakis(dimethylamido)zirconium ($Zr(NMe_2)_4$, Sigma–Aldrich) and H_2O as precursors. The coating was obtained using the reactions shown in (E) and (F) below [50].

$$\text{surface-OH} + Zr(NMe_2)_4\,(g) \rightarrow \text{surface-O–}Zr(NMe_2)_3 + HNMe_2\,(g) \quad \text{(E)}$$

$$\text{surface-O–}Zr(NMe_2)_3 + 3H_2O\,(g) \rightarrow \text{surface-O–}Zr(OH)_3 + 3HNMe_2\,(g) \quad \text{(F)}$$

The ALD coating of LiAlOx was made by combining two sequential subprocesses: Al–O followed by Li–O, in a ratio of 1:1, per deposition cycle [51]. The Al–O ALD subprocess was the same as that given in (A) and (B), above. The Li–O subprocess used lithium *tert*-butoxide ($LiOC(CH_3)_3$, Strem Chemicals) as a precursor; the reactions used are given in (G) below [52].

$$\text{surface-O–Al–OH} + LiOC(CH_3)_3\,(g) \rightarrow \text{surface-O–Al–O–Li} + HOC(CH_3)_3\,(g) \quad \text{(G)}$$

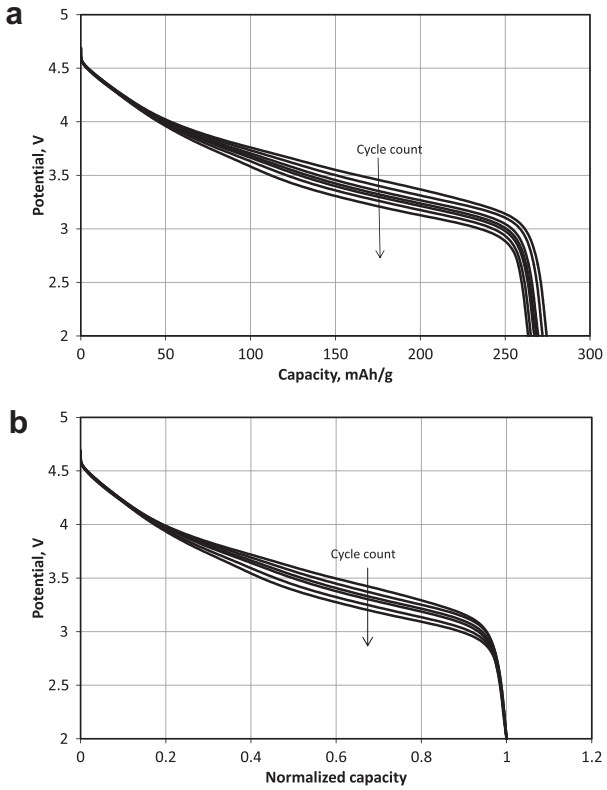

Fig. 1. a. Cell potential vs. capacity for a lithium-ion cathode containing a typical LMR–NMC material in a half cell, showing changes in voltage response with cycling at 30 °C. The data shown represent the voltage response for 20 discharge cycles; selected cycles have been removed for the sake of clarity. The cell was cycled using a ~20 mA g^{-1} current (~C/10 rate). b. Cell potential data from figure a normalized per cycle.

2.2. Single particle coatings

2.2.1. $AlPO_4$

The active cathode material was mixed with aluminum nitrate ($Al(NO_3)_2 \cdot 9H_2O$) in $(NH_4)_2HPO_4$ solution. The aluminum phosphate ($AlPO_4$) precipitate was deposited on the surface of the active material. The resulting slurry was filtered and dried in an oven at 100 °C for 12 h. The dried powder was annealed at 400 °C for 4 h before electrode fabrication [33–36].

2.2.2. LiPON

The LiPON layer was applied to the cathode powder by using RF-magnetron sputtering. The details are given in Ref. [11]. The sputtering times were 1, 2, and 3 h. Electrodes were then cast from the coated materials.

2.3. Electrolyte additives

The concentration of 3-hexylthiophene was 0.1 wt%, and that of LiDFOB (Central Glass Co., Japan), 2.0 wt% in the carbonate-based electrolyte (see Cell construction).

2.4. Cell construction

A list of cathode compositions is shown in Table 1. For each 2032 coin cell, cathode laminates were prepared with a specific active mass loading of 6–7 mg cm^{-2}. Two laminates were made for this work at Argonne. The thickness of the first was 46 μm, and the calculated final porosity was 36.1%. The thickness of was 35 μm, and the calculated final porosity was 37.1%.

The anode consisted of lithium metal. The electrolyte consisted of 1.2 M $LiPF_6$ in EC:EMC (3:7 by wt). Celgard 2325 was used as the separator. Changes to this cell chemistry are noted below.

2.5. Cell construction at NREL

A 1 M $LiPF_6$ electrolyte solution in 1:1 w/w ethylene carbonate:diethyl carbonate (Novolyte) was used. A potentiostat (VMP3, BioLogic Science Instruments) was used to perform the electrochemical measurements.

2.6. Cell cycling

All cycling (MACCOR cycler except at NREL) was performed at room temperature. All cells were cycled between 2 V and 4.7 V at 10 mA g^{-1} for the first cycle, and then between 2 V and 4.7 V (vs. Li^+/Li) at 20 mA g^{-1} for the following cycles. The cells were cycled between 2 and 4.7 V for a minimum of 20 and a maximum of 50 times. While cycling, current interrupt measurements were carried out at 3.5, 3.9, 4.3, and 4.7 V during charge and at 4.0, 3.6, 3.2, and 2.0 V during discharge. Estimates of cell resistance were calculated from the values of cell voltage and current at times t_0 and t_1, as shown in Fig. 2 using Eq. (1).

$$R = \left|\frac{v_{t_1} - v_{t_0}}{i_{t_1} - i_{t_0}}\right|, \quad (1)$$

where v_{t_1} and v_{t_0} are the cell voltages at t_1 and t_0, respectively; i_{t_1} andi_{t_0} are the respective currents.

2.7. Data reduction

The activation charge subcycle and the discharge immediately following it were omitted from further analysis in this work. After that subcycle, the energy (Wh) and capacity (A h) values were either extracted directly from the cycling data or were calculated from the raw data using Microsoft Excel®. The average voltage for a given charge or discharge subcycle was calculated as Wh/Ah. The resistance values at the first three voltages were averaged and used to correct the average voltage value for the average resistance of the cell during a given cycle. The relative change in the iR-corrected average voltage was calculated by comparing the value from the first discharge or charge subcycle to the respective value at the discharge or charge subcycle, as shown in Eq. (2).

$$\text{Rel. change in avg. voltage} = \frac{\text{Avg. voltage}_{\text{first cycle}} - \text{Avg. voltage}_{\text{last cycle}}}{\text{Avg. voltage}_{\text{first cycle}}} \quad (2)$$

These relative average voltage values then were used for plotting and subsequent analyses.

Since the range of cycle count in this experiment was large, the relative change in average voltage was calculated using the greatest cycle count that was common to all data sets. In this work, it was 20 cycles.

Table 1
Cathode compositions used in this work.

Designation	Cathode
Baseline	86 wt% HE5050 4 wt% SFG-6 graphite 2 wt% SuperP carbon black 8 wt% PVDF
AlF_3	92 wt% active material
TiO_2 (100 °C)	4 wt% C45 conductive additive
TiO_2 (150 °C)	4 wt% Solvey 5130 binder
ZrO_2 (100 °C)	
ZrO_2 (150 °C)	
$LiAlO_x$	
$AlPO_4$	86 wt% active material 4 wt% SFG-6 graphite 2 wt% SuperP carbon black 8 wt% PVDF
5 ALD cycles Al_2O_3 (120 °C)	86 wt% active material
100 ALD cycles Al_2O_3 (120 °C)	4 wt% SFG-6 graphite 2 wt% SuperP carbon black 8 wt% PVDF
LiPON (1 h)	85 wt% active material
LiPON (2 h)	7.5 wt% SuperP carbon black
LiPON (3 h)	7.5 wt% PVDF
LiDFOB (2.0 wt%)	92 wt% active material 4 wt% C45 conductive additive 4 wt% Solvey 5130 binder
3-Hexylthiophene (0.1 wt%)	92 wt% active material 4 wt% C45 conductive additive 4 wt% Solvey 5130 binder

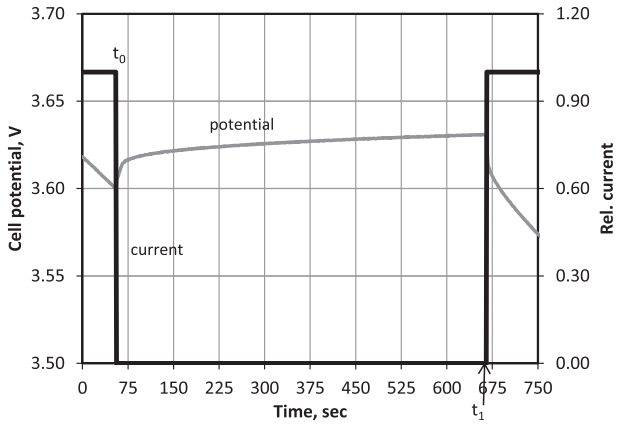

Fig. 2. Cell potential and relative current vs. time for the interrupt at 3.6 V during discharge, showing the measurement points t_0 and t_1, which were used to calculate cell resistance. The current is indicated by the heavy black line, and the voltage response of the cell, by the gray curve. t_0 occurred just before the current was turned off, and t1 occurred just before the current was turned on. The current interrupt data for the other discharge voltages and for those during the charge subcycle were treated analogously.

3. Results

3.1. General

Cell construction was found to have little-to-no effect on voltage fade. This is discussed in Ref. [53].

3.2. Capacity fade

As expected, the cell discharge capacity faded with cycling for cells containing the electrolyte additives and the coated or uncoated cathode materials, as shown in Fig. 3. The baseline showed the greatest amount of capacity fade, which was due to impedance rise and loss of active sites in the positive electrode when cycled to 4.7 V. Fig. 3 shows that the capacity fade rate of the coated materials is sensitive to the nature of the coating; some coated materials display greater capacity loss rates than others. It was interesting to note that the loss of capacity in cells containing an electrolyte additive were different, with the cell containing LiDFOB displaying about 25% of the capacity loss of the cell containing 3-hexylthiophene. Of more importance, the data in Fig. 3 clearly show that the capacity of cells containing coated cathode materials or electrolyte additives fades slower than that of the cell containing either no additive or uncoated materials. This trend is consistent with reports in the literature [8–32,37–39].

3.3. Voltage fade

In these experiments, the cells containing either coated cathodes or an additive behaved similarly as those that were uncoated or contained no additive. Examples of the aging behavior of cells containing an uncoated cathode and coated cathode are shown in Figs. 4 and 5, respectively. The first charge cycle is believed to activate the Li_2MnO_3 portion of the composite cathode material, a process needed to achieve high capacity density. With continued cycling, the cathode material loses voltage, as indicated by the changes in the voltage vs. normalized capacity curves; this loss of voltage behavior is consistent with that seen by others [3,6].

The iR-corrected, average voltage value for a given cycle was calculated using the data shown in Fig. 4. A typical average voltage vs. cycle count plot is shown in Fig. 6. The curves shown in Fig. 6 closely follow the cell voltage behavior shown in Fig. 5 for both charge and discharge. It should be noted that the shape of the average voltage curve was not sensitive to the presence of a coating or its nature, or to the presence of an electrolyte additive.

The relative change in average voltage for the cells is given in Table 2. In some cases, there was more than one cell for a given coating. This is indicated by the presence of a value for standard error (s.e.). Examining the values for the discharge subcycle shows that, after 20 cycles, most were within about 17% of the value given for the baseline material, and the value for LiPON (3 h) was almost twice that given for the baseline. The values given for the relative change in average voltage during the charge subcycle show a similar pattern after 20 cycles. Most values were within about 30% of the value given for the baseline, and that for LiPON(3 h) was twice that given for the baseline.

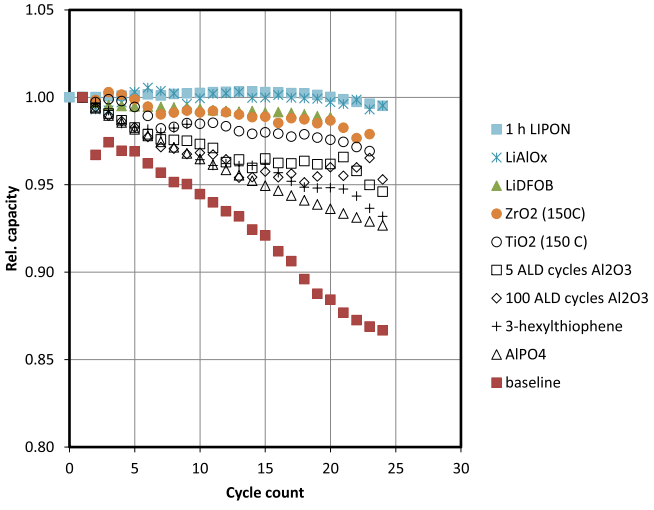

Fig. 3. Rel. cell capacity vs. cycle count, showing capacity decline with cycle count. The capacity of coated materials tended to decline slower than that of uncoated materials. The relative cell capacity vs. cycle count for the 2- and 3-h LiPON coatings behaved similarly to that seen for the 1-h coating. These data were omitted for the sake of clarity.

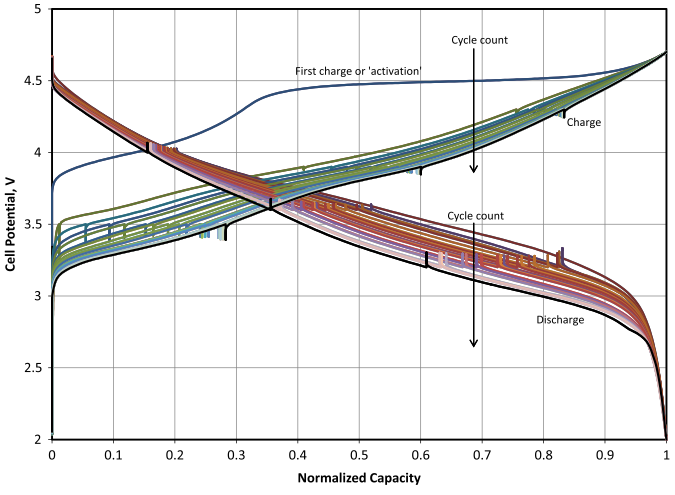

Fig. 4. Cell potential vs. normalized capacity, representing the typical charge and discharge voltage response of a cell containing an uncoated cathode in these experiments. Selected curves were removed for the sake of clarity. During the first charge, the LMR–NMC material was activated. With continued cycling, the voltage response for both the charge and discharge subcycles changed. The downward tick marks on the charge curves and upward tick marks on the discharge curves represent current interrupts.

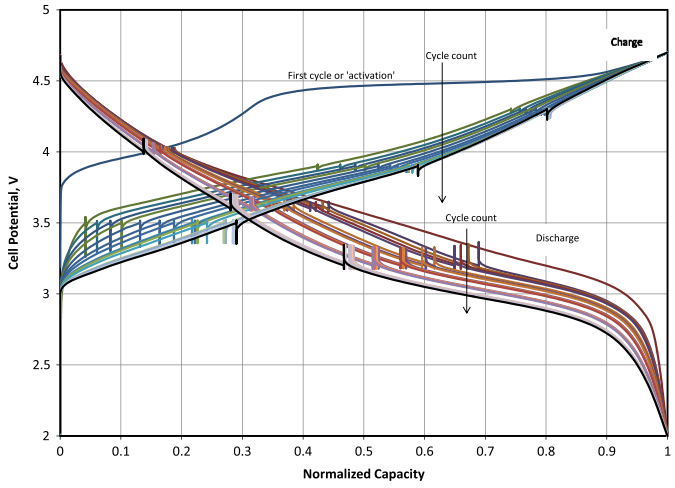

Fig. 5. Cell potential vs. normalized capacity, representing the typical charge and discharge voltage response of a cell containing a coated cathode in these experiments. Selected curves were removed for the sake of clarity. During the first charge, the LMR–NMC material was activated. With continued cycling, the voltage response for both the charge and discharge subcycles changed. The downward tick marks on the charge curves and upward tick marks on the discharge curves represent current interrupts.

It is interesting to note that neither the thickness of the Al_2O_3 layer nor the deposition temperature of the TiO_2 and ZrO_2 layers had a significant effect on the relative change in the average voltage. The voltage loss from cathodes containing $LiAlO_x$ was approximately the same as those containing TiO_2 or ZrO_2 layers.

The data in Table 2 show that the values given for the 1-h and 2-h LiPON layers were outside the statistical range for the discharge subcycles and within the statistical range for the charge subcycles. The additional hour of sputtering time did not markedly change the voltage fade response characteristic. However, at 3 h, voltage fade increased by about a factor of 2 for both the charge and discharge subcycles, which was due to the increase in electronic resistance of the LiPON film surrounding the cathode particles [13,14].

After 20 cycles, the values given for the $AlPO_4$ layer and the electrolyte additives are also outside the statistical range. The values for the electrolyte additives indicate that the average voltage decreased slightly less than the baseline. The value for $AlPO_4$ indicates that the average voltage decreased slightly more than the baseline. After 50 cycles, the values indicate a greater loss.

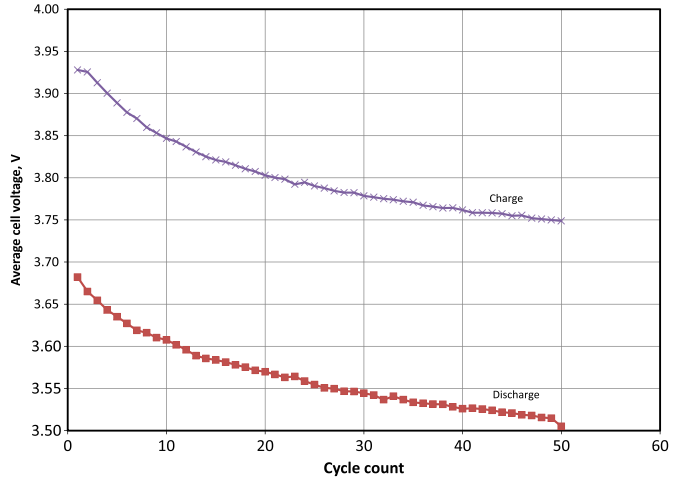

Fig. 6. Typical plot of iR-corrected average cell voltage (Wh/Ah) vs. cycle count from a baseline cell, showing that, during both charge and discharge subcycles, the average cell voltage decreases with cycling. The first cycle was omitted from this plot.

Table 2
Relative change in average voltage in baseline cells and in cells containing an electrolyte additive or a coated cathode.

Coating/additive	100 × rel. change in average voltage after 20 cycles (100 × s.e.)	100 × rel. change in average voltage after 50 cycles (100 × s.e.)
Discharge		
Baseline	3.14 (0.10)	4.81
3-Hexylthiophene	2.88	4.52
LiDFOB	3.38	
Al_2O_3 (5 ALD cycles)	3.40	5.30
Al_2O_3 (100 ALD cycles)	3.22	5.47
$AlPO_4$	3.68	5.48
$LiAlO_x$	3.32 (0.07)	
TiO_2 (100 °C)	3.14 (0.04)	
TiO_2 (150 °C)	3.20 (0.07)	
ZrO_2 (100 °C)	3.17 (0.01)	
ZrO_2 (150 °C)	3.26 (0.03)	
LiPON (1 h)	2.69	
LiPON (2 h)	2.60	
LiPON (3 h)	5.20	
Charge		
Baseline	3.97 (0.49)	4.52
3-Hexylthiophene	3.16	4.20
LiDFOB	4.89	
Al_2O_3 (5 ALD cycles)	3.52	5.15
Al_2O_3 (100 ALD cycles)	3.14	4.70
$AlPO_4$	3.66	5.03
$LiAlO_x$	5.21 (0.05)	
TiO_2 (100 °C)	4.39 (0.01)	
TiO_2 (150 °C)	4.60 (0.01)	
ZrO_2 (100 °C)	4.62 (0.02)	
ZrO_2 (150 °C)	4.85 (0.03)	
LiPON (1 h)	3.67	
LiPON (2 h)	3.75	
LiPON (3 h)	7.97	

4. Discussion

The central question underlying this work concerned the origin of voltage fade. That is, is the voltage fade phenomenon controlled by a reaction at the cathode-electrolyte interface? Theoretically, if voltage fade were caused by the loss of oxygen (e.g., during electrochemical activation [52]) or the loss of a soluble constituent, such as Mn^{2+}, changing the nature of the exposed cathode surface should change the rate at which the reaction proceeds by a significant amount.

In the literature [8–32,37–39] and in this work, coatings and electrolyte additives were shown to be very effective in controlling capacity loss. The rates of these reactions displayed significant changes in the presence of an interface-modifying organic or inorganic material. However, the results in the present work indicate that using interface-modifying materials or additives had little-to-no effect on voltage fade. Under the cycling conditions used in these experiments, voltage fade appears to derive from an intrinsic property of the LMR–NMC materials, such as thermodynamic instability, and proceeds at a rate of a few millivolts per cycle [53]. Adjusting the cycling window was found to be one practical approach to reduce voltage fade [53,54].

5. Conclusions

The effects of the coatings Al_2O_3, $LiAlO_x$, ZrO_2, TiO_2, $AlPO_4$, and LiPON and of the electrolyte additives 3-hexylthiophene and LiDFOB on the voltage fade phenomenon in $0.5Li_2MnO_3 \cdot 0.5LiNi_{0.375}Mn_{0.375}Co_{0.25}O_2$ cathodes were investigated. Cells containing these materials were cycled according to a standard protocol at room temperature. As expected, the cells containing either an additive or a coated cathode displayed less capacity loss

than cells containing an uncoated cathode and no additive. The voltage fade phenomenon was quantified in terms of the change in a resistance-corrected average cell voltage. The results indicate that, within experimental error, there was little-to-no effect on voltage fade from the coatings and additives, pointing to voltage fade being tied to the intrinsic nature of the cathode material.

Acknowledgments

The work at Argonne National Laboratory was performed under the auspices of the U.S Department of Energy (DOE), Office of Vehicle Technologies, under Contract No. DE-AC02-06CH11357. J. W. Elam and X. Meng were supported as part of the Center for Electrical Energy Storage: Tailored Interfaces, an Energy Frontier Research Center funded by the DOE, Office of Science, Office of Basic Energy Sciences. Robert Tenent and Chunmei Ban thank Dr. Peter Faguy for funding under the Applied Batteries Research (ABR) program from the Vehicles Technology Office of the DOE Office of Energy Efficiency and Renewable Energy (EERE) under DOE Agreement #24282. The research at Oak Ridge National Laboratory, managed by UT-Battelle, LLC, for the DOE under contract DE-AC05-00OR22725, is sponsored by the Vehicle Technologies Program for the EERE.

W. Lu would like to thank Drs. R. V. Bugga and W. C. West (Jet Propulsion Lab, California, USA) for providing $AlPO_4$-coated LMR–NMC. M. Bettge and D. P. Abraham would like to thank Y. Li and Dr. Y. Zhu for help with materials and experiments. L. Trahey, A. Abouimrane, I. Belharouak, X. Zhang, Q. Wu, J. W. Elam, and X. Meng would like to thank Dr. A. N. Jansen, Mr. B. Polzin, and Mr. S. Trask of the Argonne Cell Fabrication Facility for providing laminates of cathode material.

References

[1] J. Croy, K. Gallagher, M. Balasubramanian, Z. Chen, Y. Ren, S.-H. Kang, D.W. Dees, M.M. Thackeray, J. Phys. Chem. C 117 (13) (2013) 6525–6536.
[2] M.M. Thackeray, S.-H. Kang, C.S. Johnson, J.T. Vaughey, R. Benedek, S.A. Hackney, J. Mater. Chem. 17 (2007) 3112–3125.
[3] B. Xu, D. Qian, Z. Wang, Y.S. Meng, Mater. Sci. Eng. R. 73 (2012) 51–65.
[4] B. Xu, C.R. Fell, M. Chic, Y.S. Meng, Energy Environ. Sci. 4 (2011) 2223.
[5] A.R. Armstrong, N. Dupre, A.J. Paterson, C.P. Grey, P.G. Bruce, Chem. Mater. 16 (2004) 3106–3118.
[6] D. Mohanty, S. Kalnaus, R.A. Meisner, K.J. Rhodes, J. Li, E.A. Payzant, D.L. Wood III, C. Daniel, J. Power Sources 229 (2013) 239–248.
[7] M. Gu, I. Belharouak, J. Zheng, H. Wu, J. Xiao, A. Genc, K. Amine, C. Wang, ACS Nano 7 (2012) 760–767.
[8] J. Liu, Z. Chen, S. Busking, I. Belharouak, K. Amine, J. Power Sources 174 (2007) 852–855.
[9] S.S. Zhang, J. Power Sources 162 (2006) 1379–1394.
[10] Y. Kim, N.J. Dudney, M. Chi, S.K. Martha, J. Nanda, G.M. Veith, C. Liang, J. Electrochem. Soc. 160 (2013) A3113–A3125.
[11] S.K. Martha, J. Nanda, Y. Kim, R.R. Unocic, S. Pannala, N.J. Dudney, J. Mater. Chem. A 1 (2013) 5587–5595.
[12] D. Guan, Y. Wang, Ionics 19 (2013) 1–8.
[13] J.-H. Kim, M.-S. Park, J.-H. Song, D.-J. Byun, Y.-J. Kim, J.-S. Kim, J. Alloys Compd. 517 (2012) 20–25.
[14] H.-J. Kweon, S.J. Kim, D.G. Park, J. Power Sources 88 (2000) 255–261.
[15] M. Mladenov, R. Stoyanova, E. Zhecheva, S. Vassilev, Electrochem. Commun. 3 (2001) 410–416.
[16] L.A. Riley, S. Van Atta, A.S. Cavanagh, Y. Yan, S.M. George, P. Liu, A.C. Dillon, S.-H. Lee, J. Power Sources 196 (2011) 3317–3324.
[17] E.-G. Shim, T.-H. Nam, J.-G. Kim, H.-S. Kim, S.-I. Moon, J. Power Sources 172 (2007) 901–907.
[18] W.C. West, J. Soler, M.C. Smart, B.V. Ratnakumar, S. Firdosy, V. Ravi, M.S. Anderson, J. Hrbacek, E.S. Lee, A. Manthiram, J. Electrochem. Soc. 158 (2011) A883–A889.
[19] F. Wu, M. Wang, Y. Su, S. Chen, B. Xu, J. Power Sources 191 (2009) 628–632.
[20] R. Guo, P. Shi, X. Cheng, L. Sun, Electrochim. Acta 54 (2009) 5796–5803.
[21] J. Liu, A. Manthiram, J. Mater. Chem. 20 (2010) 3961–3967.
[22] J. Ni, L. Gao, L. Lu, J. Power Sources 221 (2013) 35–41.
[23] F. Wu, M. Wang, Y. Su, L. Bao, S. Chen, Electrochim. Acta 54 (2009) 6803–6807.
[24] L. Yang, B.L. Lucht, Electrochem. Solid-State Lett. 12 (2009) A229–A231.
[25] H. Zhao, L. Gao, W. Qiu, X. Zhang, J. Power Sources 132 (2004) 195–200.
[26] A. Abouimrane, S.A. Odom, H. Tavassol, M.V. Schulmerich, H. Wu, R. Bhargava, A.A. Gewirth, J.S. Moore, K. Amine, J. Electrochem. Soc. 160 (2013) A268–A271.
[27] J.C. Burns, N.N. Sinha, D.J. Coyle, G. Jain, C.M. VanElzen, W.M. Lamanna, A. Xiao, E. Scott, J.P. Gardner, J.R. Dahn, J. Electrochem. Soc. 159 (2012) A85–A90.
[28] Z. Chen, J.R. Dahn, Electrochem. Solid-State Lett. 5 (2002) A213–A216.
[29] S.-K. Hu, G.-H. Cheng, M.-Y. Cheng, B.-J. Hwang, R. Santhanam, J. Power Sources 188 (2009) 564–569.
[30] A.M. Kannan, A. Manthiram, Electrochem. Solid-State Lett. 5 (2002) A167–A169.
[31] T. Liu, S.-X. Zhao, K. Wang, C.-W. Nan, Electrochim. Acta 85 (2012) 605–611.
[32] Q. Wu, W. Lu, M. Miranda, T.K. Honaker-Schroeder, K.Y. Lakhsassi, D. Dees, Electrochem. Commun. 24 (2012) 78–81.
[33] J. Cho, T.G. Kim, C. Kim, J.-G. Lee, Y.-W. Kim, B. Park, J. Power Sources 146 (2004) 58–64.
[34] Y. Wu, A.V. Murugan, A. Manthiram, J. Electrochem. Soc. 155 (2008) A635–A641.
[35] E. Jung, Y.-J. Park, Nanoscale Res. Lett. 7 (2012) 1–4.
[36] J. Wang, Y. Wang, Y. Guo, Z. Ren, C. Liu, J. Mater. Chem. A 1 (2013) 4879–4884.
[37] M. Bettge, Y. Li, B. Sankaran, N. Dietz Rago, T. Spila, R.T. Haasch, I. Petrov, D.P. Abraham, J. Power Sources 233 (2013) 346–357.
[38] Y. Zhu, Y. Li, M. Bettge, D.P. Abraham, J. Electrochem. Soc. 159 (2012) A2109–A2117.
[39] Y. Zhu, Y. Li, M. Bettge, D. P. Abraham, Electrochim. Acta, http://dx.doi.org/10.1016/j.electacta.2013.03.102, in press.
[40] A. Abouimrane, O.C. Compton, H. Deng, I. Belharouak, D.A. Dikin, S.-B.T. Nguyen, K. Amine, Electrochem. Solid-State Lett. 14 (9) (2011) 126.
[41] Y.-H. Cho, K. Kim, S. Ahn, H.K. Liu, J. Power Sources 196 (2011) 1483–1487.
[42] C.-C. Chang, K.-Y. Lee, H.-Y. Lee, Y.-H. Su, L.-J. Her, J. Power Sources 217 (2012) 524–529.
[43] C. Li, H.P. Zhang, L.J. Fu, H. Liu, Y.P. Wu, E. Rahm, R. Holze, H.Q. Wu, Electrochim. Acta 51 (2006) 3872–3883.
[44] S. Santee, A. Xiao, L. Yang, J. Gnanaraj, B.L. Lucht, J. Power Sources 194 (2009) 1053–1060.
[45] Y. Iriyama, H. Kurita, I. Yamada, T. Abe, Z. Ogumi, J. Power Sources 137 (2004) 111–116.
[46] S.M. George, O. Sneh, A.C. Dillon, M.L. Wise, A.W. Ott, L.A. Okada, J.D. Way, Appl. Surf. Sci. 82-3 (1994) 460.
[47] Y.S. Jung, A.S. Cavanagh, A.C. Dillon, M.D. Groner, S.M. George, S.H. Lee, J. Electrochem. Soc. 157 (2010) A75.
[48] Y.S. Jung, A.S. Cavanagh, L.A. Riley, S.H. Kang, A.C. Dillon, M.D. Groner, S.M. George, S.H. Lee, Adv. Mater. 22 (2010) 2172.
[49] A. Rahtu, M. Ritala, Chem. Vap. Deposition 8 (2002) 21.
[50] D.M. Hausmann, E. Kim, J. Becker, R.G. Gordon, Chem. Mater. 14 (2002) 4350–4358.
[51] D.J. Comstock, J.W. Elam, J. Phys. Chem. C 117 (2013) 1677–1683.
[52] A.R. Armstrong, M. Holzapfel, P. Novak, C.S. Johnson, S.-H. Kang, M.M. Thackeray, P.G. Bruce, J. Am. Chem. Soc. 128 (2006) 8694–8698.
[53] M. Bettge, Y. Li, K. Gallagher, Y. Zhu, Q. Wu, W. Lu, I. Bloom, D.P. Abraham, J. Electrochem. Soc. 160 (2013) A2046–A2055.
[54] K.G. Gallagher, J.R. Croy, M. Balasubramanian, M. Bettge, D.P. Abraham, A.K. Burrell, M.M. Thackeray, Electrochem. Commun. 33 (2013) 96–98.